Elemental Germanium as a CMOS-Compatible Phase-Change Material: From Fundamental Properties to Device Demonstration

T. Zellweger*, K. Portner, C. Weilenmann, H. He, K. Bauer, A. Emboras, M. Luisier
Integrated Systems Laboratory, ETH Zurich, Switzerland
*till.zellweger@iis.ee.ethz.ch

***Abstract*—The fabrication of both established and emerging phase change memories (PCM) involves tellurium, selenium, and/or antimony, elements that are considered contaminants in standard CMOS processes. This requires dedicated tools and physically segregated process bays, adding significant cost and complexity, while limiting the widespread commercial adoption of PCM. Here, we propose elemental germanium (Ge) as an alternative PCM material. Ge is fully compatible with standard CMOS tooling and already well established in advanced technology nodes and standard foundry process flows. The potential and viability of elemental Ge as PCM material is demonstrated through in-depth investigations of its key properties and of candidate electrode materials, identifying critical requirements for a functional PCM cell. In particular, we report the realization of an elemental Ge PCM cell demonstrating threshold switching, reversible cycling, and confirm the phase-change mechanism via Raman spectroscopy. Overall, our results represent the first step towards a PCM fully compatible with standard CMOS fabrication infrastructure.**

***Index Terms*—Phase-change memory, single element, germanium, CMOS compatibility**

I. Introduction

Phase change memories (PCM) are a leading non-volatile memory technology with well-characterized device physics, offering high scalability, large resistance contrast, and multi-level storage capability [1]. $Ge_2Sb_2Te_5$ (GST) has established itself as the *de facto* standard phase change material, owing to its well-balanced combination of speed, stability, and cyclability and its proven use in commercial devices [2]. Nevertheless, alternative phase-change materials are emerging, with properties tailored for a specific application, e.g., Ge-rich GST for thermally stable embedded memory [3], (doped) Sb_2Te_3 for superior switching speed in high-speed memory [4], or recently $CrTe_3$ for minimized resistance drift in multilevel storage and neuromorphic computing [5].

However, all these phase-change materials share a common constraint: they contain tellurium, selenium, and/or antimony. These elements can act as unintended dopants or introduce deep-level defects in silicon [6], [7], and are therefore treated as contamination-sensitive species in CMOS fabrication. Hence, the fabrication of PCM cells requires dedicated tools usually physically segregated from standard CMOS equipment, which adds cost and complexity, factors critical to the commercial viability of embedded memory technologies [8]. In contrast, germanium is already native to advanced CMOS technology nodes, where SiGe alloys are widely used for strained source/drain regions and high-mobility channel engineering [9]. Moreover, elemental Ge has been monolithically integrated within the front-end-of-line (FEOL) stack [10], making it fully compatible with standard semiconductor fabrication processes.

Motivated by its CMOS-compatibility, we report, to the best of our knowledge, the first PCM cell based on purely elemental Ge, showing unipolar and reversible switching. The fabricated devices rely on a horizontal architecture that provides direct access to the switching region, enabling a thorough investigation at different resistance states. We characterize the properties of the germanium layer as novel phase-change material through resistivity, X-ray diffraction, Raman spectroscopy, and optical measurements across both the amorphous and crystalline phase. Furthermore, we assess the compatibility of candidate electrode materials with respect to metal migration. Finally, a Raman investigation of the Ge-based PCM cell before and after electrical switching to different on-state resistances is performed, confirming that the resistance changes are driven by phase transitions. This work represents a first step towards phase-change memories that are fully CMOS and back-end-of-line (BEOL) compatible.

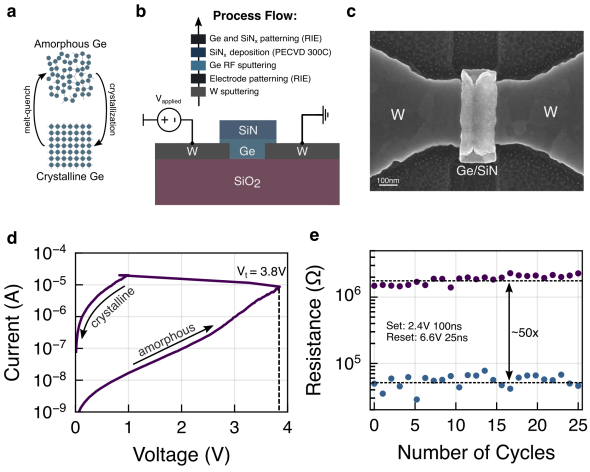

Fig. 1. Device structure and electrical characterization of the Ge PCM cell. (a) Schematic illustration of the phase-change mechanism in elemental Ge. (b) Fabrication process flow and schematic cross section. (c) SEM top-view image of the fabricated device. (d) Representative current-voltage characteristic showing threshold switching and snapback at $V_{th} \approx 3.8\,V$. (e) Reversible pulsed switching over 25 consecutive cycles using a 25 ns, 6.6 V RESET pulse and a 100 ns, 2.4 V SET pulse, with an on/off ratio of approximately 50.

II. Device Structure and Electrical Operation

Figure 1a illustrates the phase-change mechanism underlying the proposed Ge PCM cell: unlike conventional compound PCMs such as GST, elemental Ge undergoes a reversible structural transition as a single atomic species, switching between the amorphous and crystalline phase via melt-quench and crystallization, respectively. Figure 1b shows the schematic cross section and fabrication process flow of the proposed Ge PCM cell. The corresponding Scanning Electron Microscopy (SEM) top-view image of the fabricated structure is reported in Fig. 1c.

The devices are fabricated by sputtering 30 nm low-stress tungsten onto a silicon substrate with 300 nm thermal oxide. The electrodes are patterned in a two-step etching process, first forming a single wire, followed by a fine etch to introduce a 30 nm gap. After an argon clean, a 50 nm amorphous Ge layer and a 50 nm SiN_x capping layer are deposited by RF sputtering and PECVD, respectively. Both layers are subsequently etched to form a narrow region around the inter-electrode gap. All materials used are standard in CMOS fabrication, whereas the maximal thermal budget (300°C) remains well within typical BEOL limits.

Figure 1d presents a typical current-voltage measurement of our Ge PCM cells. Threshold switching and the expected snap-back behavior of phase-change memory devices are clearly visible, with a threshold voltage of approximately 3.8 V. Reversible switching through unipolar electrical pulses is demonstrated in Fig. 1e for 25 consecutive cycles, showing a clear resistance contrast between the high and low resistance states, with an on/off ratio of ∼50. These results confirm electrically-induced reversible phase-change switching in elemental Ge, validating it as a functional PCM material. Direct confirmation of the phase-change mechanism is established in Section V via Raman spectroscopy.

III. Phase-Change Properties of Elemental Ge Thin Films

To investigate the properties of germanium as a phase-change material, 100 nm Ge thin films are deposited on Si and glass substrates. First, the crystallization temperature is determined by temperature-resolved XRD. Figure 2a indicates the onset of crystallization at approximately 490°C. This value is significantly higher than conventional PCM materials such as GST (approximately 150°C [11]), making elemental Ge highly promising for thermally stable embedded memory and high data retention.

The films are then further characterized both in their amorphous (as-deposited) and polycrystalline phase (after rapid thermal annealing at 450°C for 20 min). The lower annealing temperature compared to the XRD-determined onset is sufficient to crystallize the films due to the extended duration. The amorphous films display a characteristic broad peak at 275 cm^{-1}, the polycrystalline ones a narrow peak at around 300 cm^{-1}, as depicted in Fig. 2b.

Figure 2c shows the measured film resistivity of both phases over 120 hours, fitted with the drift equation $\rho(t) = \rho_0(t/t_0)^\nu$,

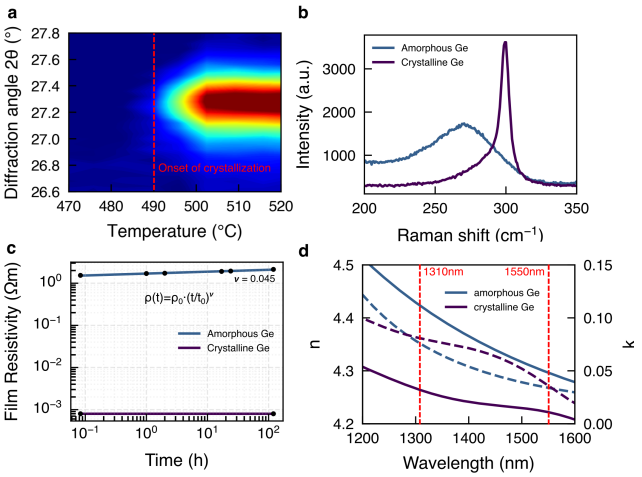

Fig. 2. Characterization of 100 nm Ge thin films. (a) Temperature-resolved XRD highlighting crystallization onset at approximately 490°C. (b) Raman spectra of the amorphous (as-deposited) and polycrystalline (RTA at 450°C, 20 min) phases, with a broad peak at 275 cm^{-1} for amorphous Ge and a sharp peak at 300 cm^{-1} for polycrystalline Ge. (c) Film resistivity measured over 120 hours, fitted with the drift equation $\rho(t) = \rho_0(t/t_0)^\nu$. A large contrast between both phases and a low amorphous-phase drift coefficient of $\nu \approx 0.045$ is observed. (d) Complex refractive index n (real, solid) and k (imaginary, dashed) of both phases determined by ellipsometry. The red dashed lines indicate the telecommunication wavelengths of 1310 and 1550 nm.

where ν is the drift coefficient. A large contrast of approximately 3 orders of magnitude can be observed between the two phases, a key requirement for PCM operation. The amorphous Ge thin film is characterized by a low drift coefficient of $\nu \approx 0.045$, indicating high structural stability. For comparison, conventional GST thin films typically exhibit drift coefficients of $\nu \approx 0.1$ [12]. The significantly lower value found in elemental Ge suggests that the amorphous phase is structurally more robust, a critical advantage for multilevel storage and analog in-memory computing applications where drift limits the achievable precision.

Beyond electronic memory, phase-change materials are also increasingly used in reconfigurable photonic devices, where a nonvolatile refractive index contrast enables programmable optical switches, photonic memories, and reconfigurable metasurfaces [13]. Figure 2d shows the complex refractive index of the amorphous and crystalline phases at the standard telecommunication wavelengths of 1310 nm and 1550 nm, as determined with ellipsometry. Amorphous Ge exhibits a refractive index of approximately 4.45 (1310 nm) and 4.3 (1550 nm), while crystalline Ge possesses a slightly lower refractive index of approximately 4.25 (1310 nm) and 4.2 (1550 nm). Both phases exhibit a low extinction coefficient of around 0.075 (1310 nm) and 0.035 (1550 nm), resulting in low optical absorption across the telecommunication wavelength range. A refractive index contrast of around Δn = 0.2 (1310 nm) and Δn = 0.1 (1550 nm) is rather small compared to GST with values closer to $\Delta n \approx 2.7$ [14], but the low optical loss in both phases is a significant advantage: absorption in the crystalline state (k = 1.49 at 1550 nm [15]) is a fundamental limitation of GST-based photonic devices [16], making Ge

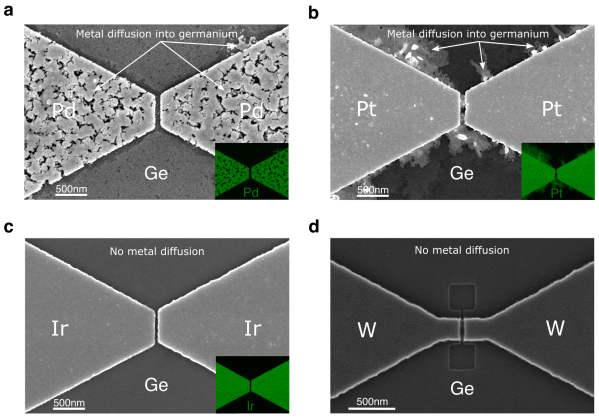

Fig. 3. Electrode compatibility study for elemental Ge PCM cells. SEM and EDX analysis of Ge/electrode interfaces after annealing at 450°C for 20 minutes are shown for (a) Pd, (b) Pt, (c) Ir, and (d) W. Pd undergoes a strong interfacial reaction with Ge, while Pt significantly diffuses into the Ge layer. Ir and W remain stable under the same conditions. For W, no EDX map is reported as the W signal overlaps with the Si signal of the substrate.

attractive for optical phase modulation. Notably, Ge is already a prominent material in silicon photonics, where it is widely deployed for high-speed photodetectors and electro-absorption modulators at telecommunication wavelengths [17]. A phase-change functionality in the same material could therefore offer unique co-integration opportunities on existing silicon photonic platforms.

IV. Electrode Compatibility Study

The electrodes represent a key building block of functional Ge PCM cells. They should not interact with Ge at the temperatures reached during device operation. While electrode stability is well-established for conventional chalcogenide PCMs such as GST, it remains to be examined for elemental Ge, which presents a distinct interfacial chemistry. Indeed, metals in contact with Ge can react and form metal-germanium compounds (germanides) that can modify the switching region or short-circuit the device across its central gap [18], [19].

To assess electrode compatibility experimentally, four chips are fabricated with the candidate electrode materials Pd, Pt, Ir, and W, with amorphous Ge deposited on top across the whole electrode region. TiN, another widely used PCM electrode, was not investigated here as it is susceptible to oxidation, which particularly in the horizontal geometry could complicate interpretation of the Ge switching behavior.

The samples are annealed at 450°C for 20 minutes, replicating a prolonged exposure to heat during device operation. SEM images of the resulting structures are shown in Fig. 3, with EDX maps of the corresponding electrode material provided as insets. The EDX map of W is omitted as it overlaps with the Si signal of the substrate.

The strongest structural change is observed for Pd, as shown in Fig. 3a. The Pd layer heavily reacts with the Ge layer above, forming a porous microstructure apparent in both the SEM image and EDX map. In the case of Pt (Fig. 3b) no pronounced reaction is observed, but a marked diffusion of Pt into Ge. The latter is also clearly visible in the EDX map. Any strong diffusion or reaction with Ge is detrimental to device performance, as it decreases cyclability and ultimately short-circuits the device. In contrast, no metal diffusion occurs with Ir or W electrodes under the same conditions (Fig. 3c and d). These observations are consistent with reported germanide formation temperatures in the literature of approximately 220°C for Pd and 340°C for Pt, while Ir germanides start forming at around 530°C, well above the 450°C investigated here. This difference may explain the absence of Ir diffusion into the germanium layer in our experiments [18]. Finally, according to the literature, W electrodes do not exhibit any sign of germanide formation up to 900°C, the highest temperature studied [18]. Consequently, tungsten was selected as the electrode material for our Ge-based PCM devices. Beyond its chemical stability with Ge, it is low-cost, well-established in CMOS processes, and already used as a standard contact plug and local interconnect metal.

V. Confirmation of Phase-Change Switching in Elemental Ge

Electrical threshold switching and reversible switching with unipolar electrical pulses are characteristic signatures of PCM operation, but alone they are not sufficient to confirm that the conductance change is driven by a structural phase transition. To provide a direct confirmation, an alternative device geometry is used, as depicted in Fig. 4a. It is largely identical to that of Fig. 1c, but with an enlarged Ge region of 5 µm, thus enabling spatially-resolved Raman spectroscopy of the switching region and a comparison to a reference signal from the surrounding unaffected Ge.

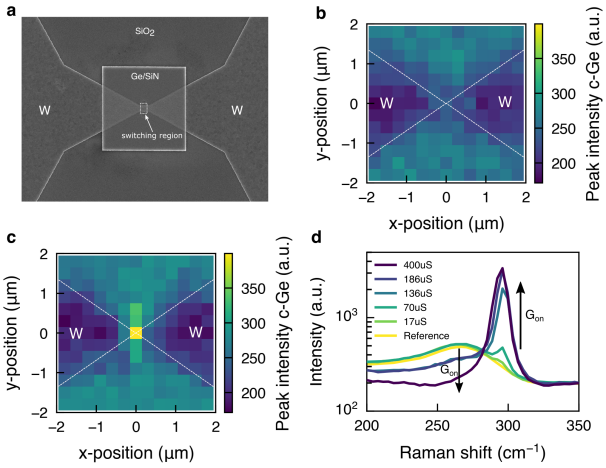

Fig. 4. Raman spectroscopic confirmation of phase-change switching in elemental Ge PCM. (a) SEM image of the device structure used for spatially resolved Raman investigation, with a Ge region of 5 µm across the gap. (b,c) 2D spatial maps of the maximum Raman intensity in the 290-300 cm^{-1} range (crystalline Ge peak) for (b) a pristine device and (c) after switching, with the W electrodes indicated by white dashed lines. A localized crystalline signal emerges in the central gap region upon electrical switching. (d) Raman spectra acquired at the gap region for different on-state conductance values between 17 and 400 µS and a pristine reference device. With increasing conductance, the crystalline Ge peak at 300 cm^{-1} grows while the amorphous Ge peak at 275 cm^{-1} simultaneously decreases, as indicated by the arrows.

Two 2D Raman maps are acquired over a $4\times4\,\mu m^2$ region centered on the gap, displaying the maximum intensity in the 290-300 cm^{-1} range corresponding to the crystalline Ge peak established in Fig. 2b. One map is acquired on a pristine, unswitched device (Fig. 4b) and one for a device after applying a voltage sweep to drive it to its on-state (Fig. 4c). In the pristine case, the map is largely homogeneous with a reduced signal over the W electrode regions due to attenuation by the underlying metal. No crystalline Raman signal is observed, confirming that the Ge layer is fully amorphous as fabricated. After switching, a distinct crystalline peak intensity emerges localized in the center of the switching gap region, directly inferring that the conductance transition induced by the voltage sweep is accompanied by a structural phase change from amorphous to crystalline Ge.

To further establish the relationship between the device conductance and the degree of crystallization, devices of the same type are switched to different on-state conductance levels ranging from 17 to 400 µS, with Raman spectra acquired for each state, and compared with a pristine reference device (Fig. 4d). A clear correlation can be observed: with increasing conductance, the crystalline Ge peak at 300 cm^{-1} grows while the amorphous Ge peak at 275 cm^{-1} simultaneously decreases, consistent with a progressive amorphous-to-crystalline phase transformation. Together, these results provide direct spectroscopic evidence that the origin of reversible electrical switching in elemental Ge PCM cells is phase change.

VI. Conclusion

In this work, we presented the realization of a phase-change memory cell based on elemental germanium, alongside a thorough investigation of the material properties and device requirements for this novel PCM. Elemental Ge thin films exhibit a resistivity contrast exceeding three orders of magnitude, a drift coefficient of $\nu \approx 0.045$, and a crystallization temperature of approximately 490°C, providing excellent thermal stability and low resistance drift of the amorphous phase. These advantageous features translate into a functional PCM cell, demonstrating threshold switching with voltage snapback and cyclable SET/RESET operation. The phase change of germanium during electrical operation was confirmed by spatially resolved Raman spectroscopy, revealing a localized crystalline Ge signal in the switching region and a clear correlation between crystalline peak intensity and device conductance. Hence, we establish elemental Ge, already widely used in advanced CMOS fabrication, as a promising new phase-change material that can be fabricated without dedicated tooling or process segregation, representing a first step towards thermally stable phase-change memories readily adoptable in existing foundry environments.

Acknowledgment

This work was supported by the SNSF Sinergia program (grant number 198612) and the Swiss State Secretariat for Education, Research, and Innovation (SERI) through the SwissChips research project. It was carried out at the Binnig and Rohrer Nanotechnology Center (BRNC) and at ETH Zurich. We thank the cleanroom operations team of the BRNC, in particular Michael Stiefel and Ute Drechsler, and the Scientific Center for Optical and Electron Microscopy (ScopeM) for their support.

References

[1] W. Zhang, R. Mazzarello, M. Wuttig, and E. Ma, "Designing crystallization in phase-change materials for universal memory and neuro-inspired computing," *Nature Reviews Materials*, vol. 4, no. 3, pp. 150–168, 2019.

[2] P. Fantini, "Phase change memory applications: the history, the present and the future," *Journal of Physics D: Applied Physics*, vol. 53, no. 28, p. 283002, 2020.

[3] A. Redaelli, E. Petroni, and R. Annunziata, "Material and process engineering challenges in ge-rich gst for embedded pcm," *Materials Science in Semiconductor Processing*, vol. 137, p. 106184, 2022.

[4] G. M. Zewdie, Y. Zhou, L. Sun, F. Rao, V. L. Deringer, R. Mazzarello, and W. Zhang, "Chemical design principles for cache-type sc–sb–te phase-change memory materials," *Chemistry of Materials*, vol. 31, no. 11, pp. 4008–4015, 2019.

[5] X. Wang, R. Wang, S. Sun, D. Xu, C. Nie, Z. Zhou, C. Wen, J. Zhang, R. Chu, X. Shen *et al.*, "Amorphous phase-change memory alloy with no resistance drift," *Nature Materials*, pp. 1–7, 2025.

[6] M. Polignano, D. Codegoni, G. Delcastello, A. Del Vitto, S. Grasso, and R. Piagge, "Tellurium contamination in silicon," *ECS Journal of Solid State Science and Technology*, vol. 2, no. 1, pp. N28–N34, 2013.

[7] H. Stümpel, M. Vorderwülbecke, and J. Mimkes, "Diffusion of selenium and tellurium in silicon," *Applied Physics A*, vol. 46, no. 3, pp. 159–163, 1988.

[8] M. Hellenbrand, I. Teck, and J. L. MacManus-Driscoll, "Progress of emerging non-volatile memory technologies in industry," *MRS communications*, vol. 14, no. 6, pp. 1099–1112, 2024.

[9] Q. Zhang, Y. Zhang, Y. Luo, and H. Yin, "New structure transistors for advanced technology node cmos ics," *National Science Review*, vol. 11, no. 3, p. nwae008, 2024.

[10] S. Assefa, F. Xia, S. W. Bedell, Y. Zhang, T. Topuria, P. M. Rice, and Y. A. Vlasov, "Cmos-integrated high-speed msm germanium waveguide photodetector," *Optics Express*, vol. 18, no. 5, pp. 4986–4999, 2010.

[11] L. Adnane, F. Dirisaglik, A. Cywar, K. Cil, Y. Zhu, C. Lam, A. Anwar, A. Gokirmak, and H. Silva, "High temperature electrical resistivity and seebeck coefficient of ge2sb2te5 thin films," *Journal of Applied Physics*, vol. 122, no. 12, 2017.

[12] M. Boniardi and D. Ielmini, "Physical origin of the resistance drift exponent in amorphous phase change materials," *Applied Physics Letters*, vol. 98, no. 24, 2011.

[13] P. Prabhathan, K. V. Sreekanth, J. Teng, J. H. Ko, Y. J. Yoo, H.-H. Jeong, Y. Lee, S. Zhang, T. Cao, C.-C. Popescu *et al.*, "Roadmap for phase change materials in photonics and beyond," *Iscience*, vol. 26, no. 10, 2023.

[14] Z. Xu, C. Chen, Z. Wang, K. Wu, H. Chong, and H. Ye, "Optical constants acquisition and phase change properties of ge 2 sb 2 te 5 thin films based on spectroscopy," *RSC advances*, vol. 8, no. 37, pp. 21 040–21 046, 2018.

[15] M. Delaney, I. Zeimpekis, D. Lawson, D. W. Hewak, and O. L. Muskens, "A new family of ultralow loss reversible phase-change materials for photonic integrated circuits: Sb2s3 and sb2se3," *Advanced functional materials*, vol. 30, no. 36, p. 2002447, 2020.

[16] Y. Zhang, J. B. Chou, J. Li, H. Li, Q. Du, A. Yadav, S. Zhou, M. Y. Shalaginov, Z. Fang, H. Zhong *et al.*, "Broadband transparent optical phase change materials for high-performance nonvolatile photonics," *Nature communications*, vol. 10, no. 1, p. 4279, 2019.

[17] D. Marris-Morini, V. Vakarin, J. M. Ramirez, Q. Liu, A. Ballabio, J. Frigerio, M. Montesinos, C. Alonso-Ramos, X. Le Roux, S. Serna *et al.*, "Germanium-based integrated photonics from near-to mid-infrared applications," *Nanophotonics*, vol. 7, no. 11, pp. 1781–1793, 2018.

[18] S. Gaudet, C. Detavernier, A. Kellock, P. Desjardins, and C. Lavoie, "Thin film reaction of transition metals with germanium," *Journal of Vacuum Science & Technology A*, vol. 24, no. 3, pp. 474–485, 2006.

[19] W. Knaepen, S. Gaudet, C. Detavernier, R. Van Meirhaeghe, J. J. Sweet, and C. Lavoie, "In situ x-ray diffraction study of metal induced crystallization of amorphous germanium," *Journal of Applied Physics*, vol. 105, no. 8, 2009.